MNRAS 000, 1–6 (2020) Preprint 17 October 2020 Compiled using MNRAS LATEX style file v3.0

High-resolution ALMA observations of V4046 Sgr: a circumbinary disc with a thin ring

Rafael Martinez-Brunner,[1]★ Simon Casassus,[1] Sebastián Pérez,[2] et al.
[1]Departamento de Astronomía, Universidad de Chile, Casilla 36-D, Santiago, Chile
[2]Universidad de Santiago de Chile, Av. Ecuador 3659, Santiago

Accepted XXX. Received YYY; in original form ZZZ

ABSTRACT

The nearby V4046 Sgr spectroscopic binary hosts a gas-rich disc known for its wide cavity and dusty ring. We present new high resolution (∼40 mas) ALMA observations of the 1.3 mm continuum. The comparison of these observations, combined with SPHERE-IRDIS polarized images and a well-sampled spectral energy distribution (SED), against radiative transfer (RT) predictions carried out with the RADMC3D package, allow us to propose a physical model for the source. The new ALMA data reveal a very fine ring at a radius of 13.46±0.43 au (Ring13), with a marginally resolved radial width of 4.17±0.94 au. Ring13 is the brightest structure in scattered-light, where it is surrounded by a ∼9 au-wide gap, and it is flanked by a very bright mm outer ring (Ring24) with a sharp inner edge at 24 au. The steeply decreasing radial slope of Ring24 breaks at ∼35 au into a shallow tail. The RT model requires an inner ring at ∼6 au (Ring6) in small dust grains, hiding under the IRDIS coronagraph, and that surrounds an inner circumbinary disk. Faint mm-continuum coincident with Ring6 is picked up by ALMA, whose morphology suggests that Ring6 is lopsided or shadowed by the secondary. The previously reported scattered-light shadow of the secondary star is also reproduced by the RT model. The surprising thin Ring13 is nonetheless 15 times wider than the model scale height, and could thus be long-lived. The strong near-far disc asymmetry at 1.65 μm points at a very forward-scattering phase function, and requires grain radii of no less than 0.4 μm.

Key words: protoplanetary discs – submillimetre: planetary systems – radiative transfer

1 INTRODUCTION

Recent observations of young circumstellar discs have transformed current knowledge of planet formation, but the focus of resolved imaging with the Atacama Large Millimeter/submillimetre Array (ALMA) or with VLT/SPHERE has mainly been towards the brighter sources (Andrews 2020). The Disks around T Tauri Stars (DARTTS) program was first presented in Avenhaus et al. (2018) with the aim to image eight stars with the Spectro-Polarimeter High-contrast Exoplanet REsearch (SPHERE). The sample is not biased towards exceptionally bright and large disks, and consists of only solar-mass stars. A second part of the survey increased the number of sources by presenting 21 new images of circumstellar disks (Garufi et al. 2020). The observations revealed diverse structures and morphologies in the scattering surface of these disks. This letter on V4046 Sagittarii (Sgr) is part of our new DARTTS survey with ALMA (DARTTS-A) which will present millimetre observations of nine protoplanetary disks previously imaged in polarized scattered light in DARTTS-S.

V4046 Sgr is a double-lined spectroscopic binary of K-type stars (K5 and K7) with very similar masses of 0.90±0.05 $M_\odot$ and 0.85±0.04 $M_\odot$ (Rosenfeld et al. 2012) on a close ($a \approx 0.041$ au), circular ($e \leq 0.001$) orbit, with an orbital period of 2.42 days (Stempels, H. C. & Gahm, G. F. 2004). It is a member of the β Pictoris moving group (Zuckerman & Song 2004), with an estimated age of 23±3 Myr (Mamajek & Bell 2014), and its distance is 72.41±0.34 pc (Gaia Collaboration et al. 2018). V4046 Sgr hosts a massive (∼0.1 $M_\odot$) circumbinary disc extending to ∼300 au (Rosenfeld et al. 2013; Rodriguez et al. 2010), with a rich observable chemical diversity (Kastner et al. 2018).

The structure of this letter is as follows. The observations, including new 1.3 mm continuum data, are described in Section 2. We interpret the data in terms of a parametric model, presented in Section 3. Previous models of V4046 Sgr have been made (Ruíz-Rodríguez et al. 2019; Rosenfeld et al. 2013; Qi et al. 2019) but our new ALMA data bring additional information. Our results are discussed in Section 4 and summarised in Section 5.

2 OBSERVATIONS

New ALMA observations of V4046 Sgr were obtained in 2017 as part of the Cycle 5 program 2017.1.01167.S (PI: S. Perez). These were acquired in the context of the DARTTS-A program (Perez et al. *in prep*), a larger survey for 9 optically visible TTauri discs at ∼50 mas resolution. The survey simultaneously mapped the 1.3 mm continuum and the J = 2−1 line of ^{12}CO with the C43-8 array configuration in band 6 (211-275 GHz). This work focuses exclusively on the data obtained in the 1.3 mm continuum for our source, taken

★ E-mail: rmartinezbrunner@gmail.com

with a beam size of 0.″04 × 0.″06 (in natural weights). **Seba, sure that the survey only used C43-8?***

In this investigation, we use the polarimetric image at 1.65 μm previously published as part of the DARTTS-SPHERE I survey (Avenhaus et al. 2018). The image was taken at the ESO Very Large Telescope with the SPHERE-IRDIS instrument in differential polarization imaging (DPI) mode, and a complete description of the data reduction was presented in Avenhaus et al. (2018).

For our analysis of the ALMA image we used an image reconstruction strategy, using the non-parametric image synthesis of the `uvmem` package (Casassus et al. 2006; Cárcamo et al. 2018) it is possible to super-resolve the clean beam, obtaining an effective angular resolution ∼3 times finer than natural weights. The model image is obtained by fitting the data using Chi-squared minimisation, with a measure of regularization when required. Here we adopted a χ^2 model image with $\lambda = 0.1$ for regularization. The resulting `uvmem` image shown in Fig. 1 exhibits previously unseen substructure of the disc. This image reveals that the disc features two rings of large dust grains with a broad gap between them, i.e. Ring13 at 13 au and Ring24 starting at 24 au. The wide and bright Ring24 reaches its peak intensity at ∼30 au, beyond which it drops steeply before breaking at ∼35 au into a shallow tail. While this is the first observation of Ring13, Ruíz-Rodríguez et al. (2019) did anticipate its existence as their ALMA continuum image showed a distinct excess between ∼10 and 17 au.

Ring13 is surprisingly narrow and seems to be off-centre relative to the GAIA stellar position (at the origin of coordinates in Fig. 1). We determined the ring's centre and orientation by minimising the dispersion of the disc radial profiles, from 6 au to 19 au, and thus obtained a PA of 74.64±0.08 °, an inclination of 33.90±0.04 ° and a centre at $\Delta\alpha = 9 \pm 0.05$ mas $\Delta\delta = 0.06 \pm 0.04$ mas, relative to the stars.

The ring width can be measured in polar coordinates by fitting 1-D Gaussians, thus obtaining a width and centroid at each azimuth. On average, we obtained a FWHM of 4.17±0.94 au, and a stellocentric radius of 13.46±0.43 au (See Fig. 2). As the `uvmem` model image has an effective angular resolution of ∼1/3 that of the natural-weighted beam (0.″04 × 0.″06), we see that Ring13 is marginally resolved. After subtraction of the approximate `uvmem` resolution (∼ 0.″01 × ∼ 0.″02), the ring width is ∼3.99±0.94 au.

Repeating the optimization of the disk orientation, but this time aiming for Ring24 with a radial domain from 20 au to 70 au, we obtained a PA of 76.78±0.03 °, with an inclination of 34.01±0.01 ° and a centre at $\Delta\alpha = 19 \pm 0.04$ mas $\Delta\delta = 7 \pm 0.03$ mas relative to the stars. We see that both Ring13 and Ring24 both share the same orientation and centre, given the errors, and both are offset from the star. Even though all orientation parameters for Ring13 and Ring24 are consistent within the errors, there are however some hints for a different orientation, as summarised in Fig. 2, perhaps due to the joint effect of all these small differences.***

Interestingly, the ALMA image also detects faint 1.3 mm continuum emission near the stellar positions (See the inset in Fig. 1). Since this faint central emission is offset from the star, at the origin of coordinates in the figure, it is probably due to large dust grains. This dust structure is at a distance of only ∼ 0.″02 from the binary system, and may match the small grain ring called Ring6 introduced in the RT model to match the SED (see Sec. **??** below). If so, then given that the binary phase at the time of the observations is PA=***, so that the secondary lies roughly northwards of the primary, it may be that the northern side of Ring6 is shadowed, resulting in a seemingly lopsided geometry.

The scattered-light image shown in Fig. 1 also shows a double ring structure in the micron-sized dust distribution. The observed morphology presents an inner cavity of ∼10 au in radius and two rings located at 14.10±0.01, coincident with Ring13, and 24.62±0.08 au, coincident with Ring24, with a small gap between them at ∼20 au. The observed second ring matches the inner wall of the 1.3 mm continuum emission outer ring (Ruíz-Rodríguez et al. 2019). Two other important features that are present in the image are: the brightness asymmetry and the shadows projected on the disc produced by the close binary system as they eclipse each other, described in detail by D'Orazi et al. (2019).

The binary phase reported by D'Orazi et al. (2019) in the scattered-light observation is at a position angle (PA) of 360-106 °, east of north. Using this measurement, the binary phase was calculated at the time of the ALMA observation at a PA of 360-13 °. There is no hint of radio decrements in either Rings13 nor in Ring24 that would match shadowing at this PA, could be explained by inefficient disk cooling compared to the speed of the illumination pattern (Casassus et al. 2019).

3 PARAMETRIC RADIATIVE TRANSFER MODEL

The multi-frequency data can be interpreted in terms of a physical structure using radiative transfer predictions, for which we used the RADMC3D package(Dullemond et al. 2012). The general framework of the parametric model that we used is similar to that in Casassus et al. (2018) for DoAr 44, and the initial model values were inspired from those in Rosenfeld et al. (2013).

For the representation of the stars, we used two Kurucz photospheres models (Kurucz 1979; Castelli et al. 1997) with $T_{\rm eff,1} = 4350$ K, $R_{*,1} = 1.064\,R_\odot$, $M_{*,1} = 0.90\,M_\odot$ and $T_{\rm eff,2} = 4060$ K, $R_{*,2} = 1.033\,R_\odot$, $M_{*,2} = 0.85\,M_\odot$ respectively and with an accretion rate of $\log \dot{M} = -9.3\,M_\odot\,{\rm yr}^{-1}$ for both cases (Donati et al. 2011). The stars were placed at a mutual separation of 0.041 au, so that their center of mass coincides with the origin, and oriented at a PA of ***** 30 °, so that the secondary lies to the NWW from the primary, thus casting the same shadow as observed by d'Orazzi**** rotation, relative to the semi-major axis of the disk, to match the shadows reported by D'Orazi et al. (2019) **** GIVE ORIENTATION IN TERMS OF THE PA****

Reproducing the radial and vertical structure of the V4046 Sgr disc turned out to be challenging. We built the model in terms of the gas distribution, and with two different dust populations: larger grains that are vertically settled and dominate the total dust mass and a population of smaller grains that are uniformly mixed with the gas and reach larger heights above the mid-plane.

Assuming a three dimensional model in a spherical reference frame with coordinates (r, θ, z), the gas density ($\rho_{\rm gas}$) distribution follows

$$\rho_{\rm gas}(r,z) = \frac{\Sigma(r)\,\delta(r)}{\sqrt{2\pi}\,rH(r)} \exp\left[-\frac{1}{2}\left(\frac{z}{rH(r)}\right)^2\right], \qquad (1)$$

where $\delta(r)$ parameterises the density drops in the gaps and cavities, $H(r)$ is the scale height profile and $\Sigma(r)$ is the surface density profile. $\Sigma(r)$ is defined by

$$\Sigma(r) = \Sigma_{\rm c}\left(\frac{r}{R_{\rm c}}\right)^{-\gamma} \exp\left[-\left(\frac{r}{R_{\rm c}}\right)^{2-\gamma}\right], \qquad (2)$$

where R_c is a characteristic radius and γ is the surface density gradient. A fixed $\gamma = 1$ is used as it is a typical value for discs (Andrews et al. 2009, 2010).

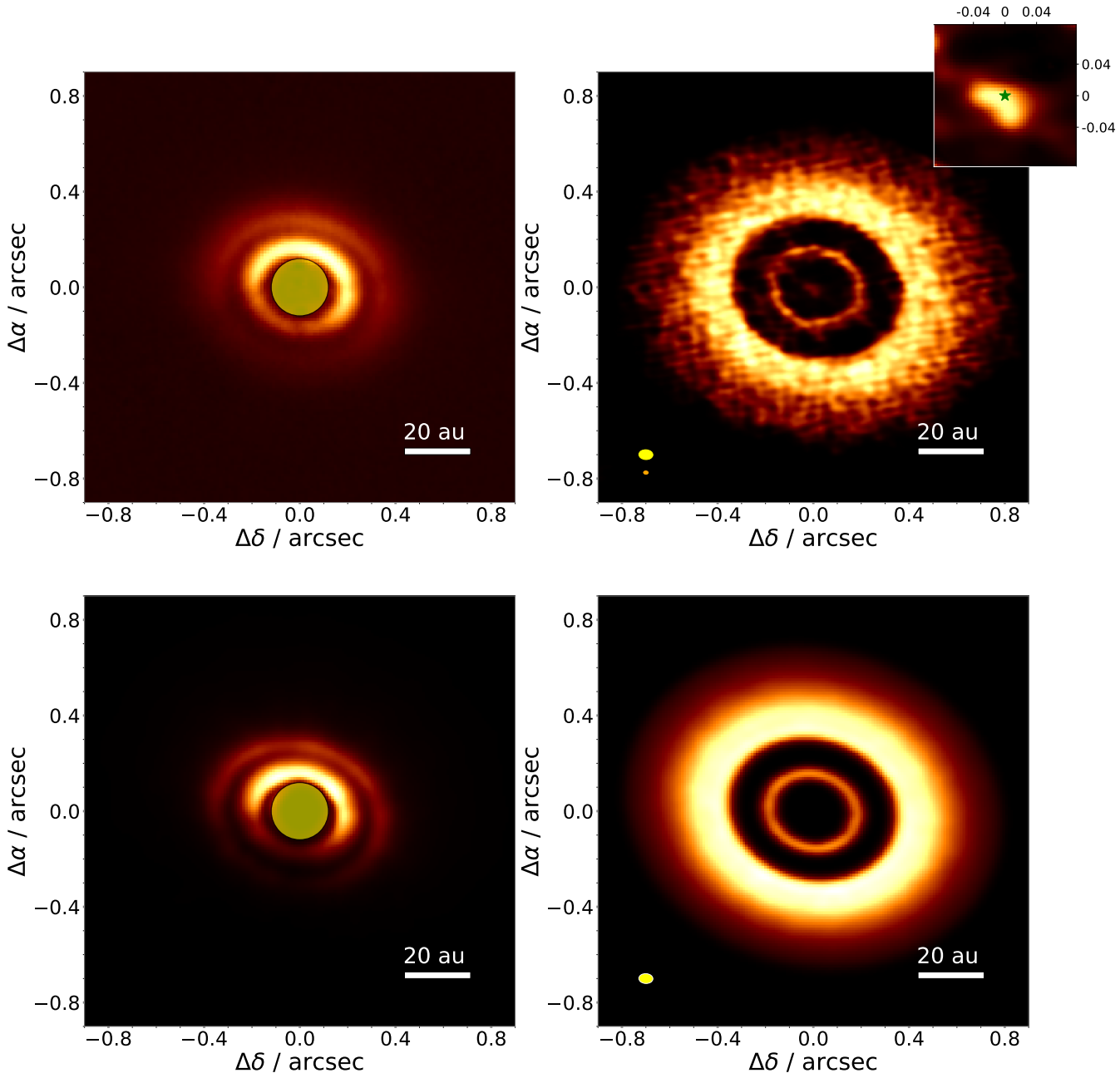

Figure 1. Comparison of observations and simulated images at 1.65 μm and 1.3 mm continuum of the circumbinary disc orbiting V4046 Sgr. From top to bottom: DPI image and ALMA Band 6 observations; simulated images of the parametric model. Top left panel: SPHERE-IRDIS H-band image with a yellow filled circle that illustrate the N_ALC_YJH_S coronagraph (inner working angle ~ 0.″12, or ~8.6 au at 72.4 pc). Top right panel: 1.3 mm continuum `uvmem` model image. The yellow ellipse shows the size of the natural-weighted beam (0.″04 × 0.″06), and the small orange ellipse shows an estimated `uvmem` beam size (~ 0.″01 × ~ 0.″02). The inset zooms into the central emission, and the green star marks the star positions. Bottom left panel: 1.65 μm simulated image of the parametric model. Bottom right panel: 1.3 mm simulated image of the parametric model. The yellow ellipse shows the size of the beam: 0.″04 × 0.″06. For all the images in the figure the colour scale is linear.

The parametric scale height profiles for the gas and for each dust population are

$$H(r) = \chi\, H_o(r)\, [r/r_o(r)]^{\psi(r)}, \qquad (3)$$

where $H_\circ$ is the scale height at r = $r_\circ$, ψ is the flaring index and χ is a scaling factor (in the range 0 – 1) that mimics dust settling. For the gas and the small dust grains χ = 1 and for the millimetre-size dust population we assign a fixed χ = 1/2 for simplicity, as in Rosenfeld et al. (2013).

For the vertical structure, D'Orazi et al. (2019) found flaring angles of φ = 6.2±0.6 ° for the inner ring and φ = 8.5±1.0 ° for the outer one. ***explicar que es varphi y como se transforma en psi**** Our

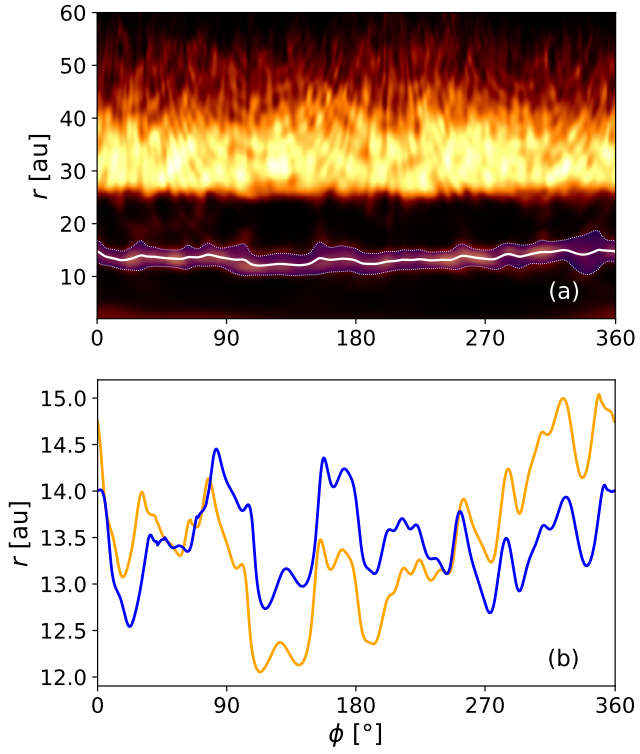

Figure 2. (a) Polar decomposition of the 1.3 mm continuum image, using the orientation of Ring24. We trace Ring13 using the centroids (solid line) and width of radial Gaussian fits (blue region between the dotted lines). (b) Centroid of Ring13, for two disc orientations: the orange line corresponds to the same trace as in a), while the blue line is obtained for the inner ring orientation.

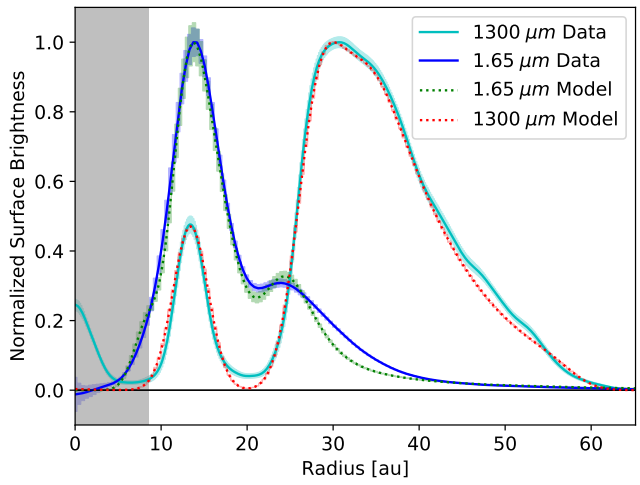

Figure 3. Comparison of the surface brightness profiles extracted from the deprojected synthetic images and observed H-band and 1.3 mm continuum images. The grey shaded area represents the inner working angle of the artificial coronagraph used in the simulations (i.e., $\sim$ 0.″12, or $\sim$8.6 au at 72.4 pc).

model uses the same values, with two different flaring indeces ψ. The separation between the two values was set at r = 19 au with ψ = 0.2 for Ring6 and Ring13, and ψ = 0.5 for Ring24. The scale height is $H_\circ$ = 0.045 at r_0 = 19.5 au.

The small-dust density distribution follows the same behaviour as the gas, with a dust-to-gas mass ratio ζ = 0.047 (as in Rosenfeld et al. 2013), the mass fraction between small and large dust particles $f_{\rm sd}$ = * * * and another factor for fine tuning that depends on the radius, $\delta_{\rm sd}(r)$. The small dust density is thus given by

$$\rho_{\rm small-dust}(r,z) = \rho_{\rm gas}(r,z)\, f_{\rm sd}\, \delta_{\rm sd}(r)\, \zeta. \quad (4)$$

***I changed $f_{\rm sd}$ to $f_{\rm sd}$. say how much is f_{sd}.

Since the large-dust grains are less coupled to the gas, their distribution has some important differences that require a special parameterisation, with a large inner cavity and scaling factors that account for the larger gap between the rings. For the inner ring, the same profile as the gas is used, but with different values for R_c and Σ_c. The greatest difference is in the outer ring, where we used a decaying power law modulated by the sum of two Gaussian profiles. In an effort to recreate the break seen in the outer ring between 32 and 34.5 au, we chose a different value for γ = -8. For the large dust grains the surface density profile is thus

$$\Sigma_{\rm large-dust}(r) = \Sigma_{\rm c2} \left(\frac{r}{R_{\rm c2}}\right)^{-\gamma} \left\{\exp\left[-\left(\frac{r}{R_{\rm c2}}\right)^{2-\gamma}\right] + \exp\left[-\left(\frac{r}{R_{\rm c2}}\right)^{2}\right]\right\}. \quad (5)$$

REWORD PARA, IT IS NOT CLEAR WHERE DOES THIS EPSILON ENTERS - IF IT IS COMMON TO BOTH SPECIES, THEN INCLUDE IT IN THE GAS PROFILE. I DID NOT CHECK REDACTION, MAKE THIS AS COMPACT AS POSSIBLE Also for both dust populations, the inner part of the outer ring follows a different behaviour. The surface density profile is multiplied by an additional factor

$$\epsilon(r) = \delta + (1-\delta)\left(\frac{r - R_{\rm in}}{R_{\rm peak} - R_{\rm in}}\right)^3, \quad (6)$$

where $\delta = 10^{-4}$ and $R_{\rm in}$ and $R_{\rm peak}$ would depend on the dust population, marking the beginning and the maximum density peak of the outer ring. This parameter allow us to model a smoother inner wall of the outer ring.

The two different populations of dust grains corresponds to the small grains, with radii ranging from 0.4 to 1.5 μm, and the large dust grains range, with radii from 0.4 μm to 10 mm. We computed the dust opacities using the `bhmie` code, with a mix composed of 70% silicate and 30% graphite.

The observed near-far asymmetry in the DPI image is suggestive of a strongly forward-scattering phase function. In order to reproduce a similar asymmetry, we required much larger grains that typically used in the RT modeling of such near-IR data (e.g. Casassus et al. 2018).

The simulated DPI image at 1.65 μm in Fig. 1 was obtained with the scattering matrix calculated by the `makeopac.py` script provided in the RADMC3D package. We used a Gaussian size distribution centred at 0.4 μm, and smeared out by 30% in both directions, and using 20 grain size bins within that range.

Through trial and error, we found a set of values for the parameters that correctly fit the available data. The final structure of the parametric model goes as Fig. 4 shows. The inner radius of the model grid was set to 0.1 au and an outter radius of 115 au, large enough for the dust disc to become undetectable.

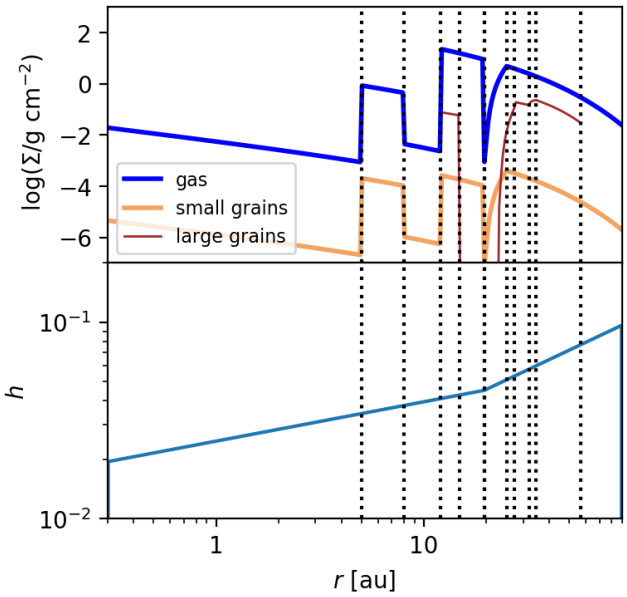

Figure 4. Top: surface density profiles for the gas, the large and small grain populations. **Bottom:** scale height profile $h(r)$. The dashed lines crossing both panels correspond to transition radii in the parametric model.

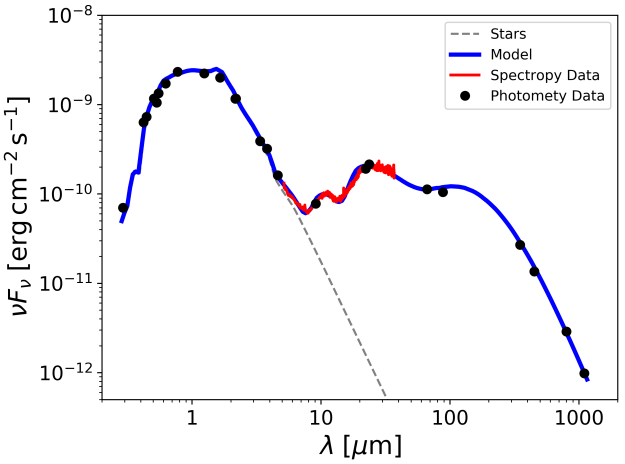

Figure 5. The observed SED of V4046 Sgr (black points and solid red curve) compared with the model (blue). The black points represent the measured photometry and the red line shows an archival *Spitzer* IRS spectrum. The dashed silver curve shows the emission of the stellar photosphere model.

The gas and small dust surface density profiles begin at 0.3 au, out of the zone expected to be cleared by dynamical interactions with the central binary (Artymowicz & Lubow 1994), which is expected to be ∼****. For the small dust grains, we propose a three ringed structure. The innermost ring of the model is located from 5 to 8 au, this ring, introduced as Ring6 in Sec. 2, is not detectable in the IRDIS observations but was required to account for the SED. Then follow the two rings observed by IRDIS: Ring13, from 12 to 19.5 au, which is surrounded by very narrow 1 au-wide gap, and then Ring24, that starts 20.5 au and has its maximum density peak at 25 au. The small-dust density then decays exponentially with radius.

On the other hand, in order to reproduce the double-ringed morphology of the millimetre continuum emission, we required a model with a wide central cavity (r = 12.3 au), a narrow 2.6 au-wide inner ring (which is Ring13) followed by a 8.2 au gap that separates the outer ring (Ring24), which starts at 23 au and reaches peak densities at 27.3 au. This last ring has an observed break between 32 and 34.5 au, which is reproduced in the model with the a discontinuity in the exponent γ, along with the sum of the decaying exponentials. We also truncated the model large-grain density at ∼57 au.

We set the values of the inclination an the position angle as the same as those obtained from the ALMA observation in Section 2, so the model has an inclination of i = 33.9 ° and a P.A. = 74.6 °. Finally, the distance is set at d = 72.4 pc (Gaia Collaboration et al. 2018).

4 MODEL RESULTS AND DISCUSSION

Our parametric model is fairly successful in reproducing the available data. The simulated images and the SED of the model are shown in Fig. 1 and Fig. 5 respectively.

The simulated image at 1.65 μm shows a similar radial structure to the one visible in the observations, displaying a two ringed disc, where Ring6 hides under the artificial coronagraph. The visible asymmetry in the SPHERE observations is recreated using grains larger than 0.4 μm as smaller grains do not cause a strong forward scattering, meaning that the disc is depleted of very-small grains. Interestingly, the model accurately shows the shadows described by D'Orazi et al. (2019) that are present in the SPHERE-IRDIS image.

The simulated 1.3 mm continuum image reproduces the two observed rings: the faint Ring13 and the brighter Ring24. As the radial profiles obtained from the simulated images of the model closely resemble those deduced from the observations (Fig. 3), we can assume that the model provides an approximation of the disc structure, including the dimensions of Ring13. Accordingly, taking the parametric model values for Ring13 we have that it has a radius of 13.6 au, a width of 2.6 au, and a scale height ranging from 0.25 to 0.32 au. The total dust mass of Ring13 is about 3 $M_\oplus$ in the model. In turn, in our model Ring24 reaches peak intensity at ∼30 au, then breaks at ∼35 au, as in the observations, and has a total dust mass of ∼43 $M_\oplus$.

****DISCUTIR EL ANCHO OBSERVADO VS. ANCHO MODELO****

As Dullemond et al. (2018) explains, the stability of a narrow dust ring requires that its height be smaller than its radial extent ***HOW MUCH SMALLER?***. Using the parametric model scale height of 0.28 au at 13.46 au and the measured width of Ring13 (4.17 au FWHM, see Section 2), we have that its width is ∼15 times its scale height.

CHECK THAT THE RT PREDICTIONS USE THE SAME BEAM FOR CONVOLUTION AS THE DATA, AND UPDATE ALL FIGURES*

The observed SED was collected from data in Jensen & Mathieu (1997), in VIZIER ***FOR WHICH BANDS?*** and DIANA ***idem***, and also using spectrometry data from an archival *Spitzer* IRS spectrum. ***THIS SHOULD GO IN SEC. OBS****

The observed SED is compared with the model in Fig. 5. From the similarity with the data we propose that there has to be a small-grain population close to the stars down to 0.3 au. The decision of employing the three ringed structure for the small dust grains relies on the fact that the SED needed a ring at a radius smaller than 10 au to have a proper fit ***WHERE in LBDA?****, and we may have detected this ring in the ALMA image, if this ring is lopsided or shadowed by the secondary.

5 CONCLUSIONS

New ALMA 1.3 mm continuum imaging of the circumbinary disc around V4046 Sgr were analysed in the context of the available IR imaging and the observed spectral energy distribution using a RT model. The key conclusions are as follows.

(i) We report the detection of a narrow ring in the 1.3 mm continuum, with a radius 13.46±0.43 au and an estimated width of 4.17±0.94 au **UPDATE FOR NEW BEAM***. The location of this ring is coincident with the inner ring observed in the scattered-light image, revealing that the ring includes around 3 $M_{\oplus}$ millimetre-sized grains. Using the parametric model scale height value (h = 0.28 au at 13.46 au) we have that the ring width is ∼15 times its estimated height ***UPDATE****

(ii) The 1.3 mm outer ring, that starts at ∼23 au and has its peak intensity at ∼32 au, presents a visible break in the surface brightness at ∼35 au.

(iii) We interpret the asymmetry observed with SPHERE-IRDIS at 1.65 μm as due to strong forward-scattering, which implies that the dust population is depleted of grains smaller than ∼0.4 μm.

(iv) Our parametric model, which accounts for the SED of the system, involves the existence of a sub-micron dust population close (<5 au) to the stars ***IS THIS NOT A CONFIRMATION OF THE INNER DIST PROPOSED BY ROSENFELD+? IF SO, SAY SO****. We also predict the existence of another thin ring at ∼6 au, about 3 au-wide and made of small dust grains, and that lies under the coronagraph of the scattered-light image. The weak central emission at 1.3 mm could be part of this ring.

ACKNOWLEDGEMENTS

Try to keep it short.

DATA AVAILABILITY

REFERENCES

Andrews S. M., 2020, arXiv e-prints, p. arXiv:2001.05007
Andrews S. M., Wilner D. J., Hughes A. M., Qi C., Dullemond C. P., 2009, The Astrophysical Journal, 700, 1502
Andrews S. M., Wilner D. J., Hughes A. M., Qi C., Dullemond C. P., 2010, The Astrophysical Journal, 723, 1241
Artymowicz P., Lubow S. H., 1994, ApJ, 421, 651
Avenhaus H., et al., 2018, The Astrophysical Journal, 863, 44
Cárcamo M., Román P. E., Casassus S., Moral V., Rannou F. R., 2018, Astronomy and Computing, 22, 16
Casassus S., Cabrera G. F., Förster F., Pearson T. J., Readhead A. C. S., Dickinson C., 2006, ApJ, 639, 951
Casassus S., et al., 2018, MNRAS, 477, 5104
Casassus S., Pérez S., Osses A., Marino S., 2019, MNRAS, 486, L58
Castelli F., Gratton R. G., Kurucz R. L., 1997, A&A, 318, 841
D'Orazi V., et al., 2019, Nature Astronomy, 3, 167
Donati J.-F., et al., 2011, Monthly Notices of the Royal Astronomical Society, 417, 1747
Dullemond C. P., Juhasz A., Pohl A., Sereshti F., Shetty R., Peters T., Commercon B.; Flock M., 2012, The Astrophysical Journal
Dullemond C. P., et al., 2018, ApJ, 869, L46
Gaia Collaboration et al., 2018, A&A, 616, A1
Garufi A., et al., 2020, A&A, 633, A82
Jensen E. L. N., Mathieu R. D., 1997, AJ, 114, 301
Kastner J. H., et al., 2018, The Astrophysical Journal, 863, 106
Kurucz R. L., 1979, ApJS, 40, 1
Mamajek E. E., Bell C. P. M., 2014, Monthly Notices of the Royal Astronomical Society, 445, 2169
Qi C., et al., 2019, ApJ, 882, 160
Rodriguez D. R., Kastner J. H., Wilner D., Qi C., 2010, The Astrophysical Journal, 720, 1684
Rosenfeld K. A., Andrews S. M., Wilner D. J., Stempels H. C., 2012, The Astrophysical Journal, 759, 119
Rosenfeld K. A., Andrews S. M., Wilner D. J., Kastner J. H., McClure M. K., 2013, The Astrophysical Journal, 775, 136
Ruíz-Rodríguez D., Kastner J. H., Dong R., Principe D. A., Andrews S. M., Wilner D. J., 2019, The Astronomical Journal, 157, 237
Stempels, H. C. Gahm, G. F. 2004, A&A, 421, 1159
Zuckerman B., Song I., 2004, Annual Review of Astronomy and Astrophysics, 42, 685

This paper has been typeset from a TEX/LATEX file prepared by the author.